Formation of bimetallic FeBi nanostructured particles : investigation of a complex growth mechanism

J. G. Mattei,[†] F. Pelletier,[‡] D. Ciuculescu,[‡] P. Lecante,[†] J.C. Dupin,[¶] N. Yaacoub,[§] J. Allouche,[¶] J. M. Greneche,[§] D. Gonbeau,[¶] C. Amiens,[‡] and M.J. Casanove[*,†]

CEMES, CNRS UPR 8011, Université de Toulouse, 29 rue Jeanne Marvig, F-31055 Toulouse, France, Université de Toulouse ; UPS ; LCC (Laboratoire de Chimie de Coordination, UPR CNRS 8241) 205 route de Narbonne F-31077 Toulouse, France, Université de Pau et Pays Adour, CNRS, IPREM, ECP,UMR 5254, F-64053 Pau 09, France, and LUNAM, Université du Maine, Institut des Molécules et Matériaux du Mans, IMMM UMR CNRS 6283, F-72085 Le Mans, France

E-mail: casanove@cemes.fr

[*]To whom correspondence should be addressed

[†]CEMES, CNRS UPR 8011, Université de Toulouse, 29 rue Jeanne Marvig, F-31055 Toulouse, France

[‡]Université de Toulouse ; UPS ; LCC (Laboratoire de Chimie de Coordination, UPR CNRS 8241) 205 route de Narbonne F-31077 Toulouse, France

[¶]Université de Pau et Pays Adour, CNRS, IPREM, ECP,UMR 5254, F-64053 Pau 09, France

[§]LUNAM, Université du Maine, Institut des Molécules et Matériaux du Mans, IMMM UMR CNRS 6283, F-72085 Le Mans, France

Abstract

Magnetic bimetallic Fe-Bi composites, synthesized by decomposition of organometallic precursors under amine borane and dihydrogen, formed regular nanospheres with mean diameter of 150 nm $\pm$ 30 nm. The nanospheres display a core-shell like chemical distribution in which bismuth is mainly concentrated in the core, as demonstrated through elemental mapping x-ray energy dispersive spectroscopy while the shell is formed by aggregated 3nm wide iron nanoparticles. The close environment of the different elements was analyzed through complementary techniques such as extended x-ray absorption fine structure, wide-angle x-ray scattering, ^{57}Fe Mössbauer and x-ray photoelectron spectroscopies. Despite their iron-rich shell, the Fe-Bi nanospheres present both good magnetic properties and enhanced resistance to oxidation during air exposure. In order to uncover the growth mechanisms leading to the formation of this compound, a series of samples taken at different steps of the synthesis process was analyzed. The role of metallic iron to promote the reduction of the bismuth precursor from the early stages of the synthesis is emphasized. Remarkably, this process promotes the formation of a metastable Fe-Bi nanoalloy.

Keywords : Bimetallic nanoparticles; bismuth; iron; growth mechanisms; structure; soft chemistry

Introduction

Nanosciences and related technologies have recently focused an important research effort on the fabrication and study of multicomponent and hybrid particles.[1] The presence of discrete domains of different materials in a same particle is indeed highly desirable for many potential applications: on the one hand, it offers the remarkable advantage of combining different properties in a single object, on the other hand it opens a route to new properties and novel functions.[2–4]Among multicomponent particles, the ones with core-shell geometry are highly valuable because the core material is effectively protected from the environment by the shell, while the shell material can

provide enhanced properties, either optical[5] or magnetic,[6] to the core-shell system. A great attention has been paid to the combination of iron with a non ferromagnetic metal in a single particle. In these materials, the use of a metal presenting a large miscibility gap with iron is particularly appealing to create core-shell chemical distribution. Several experimental or theoretical studies have thus been dedicated to the Fe/Au system in which Fe is expected to remain at the core of the particle.[7–10]

In the present paper, we focus on the iron-bismuth system in which both metals display very different properties and present a large miscibility gap. While α-Fe is ferromagnetic, bismuth behaves as a semi-metal with unique electronic properties. In particular, remarkable transport and thermoelectric properties have been reported in bismuth nanoscaled materials or nanocomposites.[11–14] Very few studies have been dedicated to the immiscible Fe-Bi system and all of them concerned thin films, either Fe/Bi multilayered films[15] or Fe-Bi bimetallic films grown by co-sputtering of elemental targets or dual electron-beam evaporation or even through ion mixing in previously grown Fe/Bi multilayered films.[16–18] In a preliminary study, we developped a successful synthesis of FeBi bimetallic nanocomposites, although the assembly of particles was not fully homogeneous.[19] In the present paper, we developped further the synthesis in the presence of hexamethyldisilazane (HMDS), which allowed the formation of bimetallic nanocomposites, so as to control the formation of an assembly of identical FeBi particles, required to perform a thorough structural and chemical analysis of the synthesized particles. Typically, we used a Fe/Bi atomic ratio as small as 7/1 instead of 1/1 as in,[19] with the aim to avoid the nucleation and growth of pure bismuth nanocrystals. Excess HMDS (namely 10 equivalent versus metal content) was used to compensate for the high lability of this amine and ensure stabilization of the colloidal solution. As our samples grow in mild conditions of temperature and pressure, and are surrounded by ligands, their structure and morphology can be very different from those expected from thermodynamics. On the contrary, kinetics can play a rather important part, as we observed in the Fe-Rh system.[20] Thorough examination of the structural and chemical features, from the core to the surface of the particles, is thus mandatory if one aims at explaining the properties of such complex

compounds. For these reasons, we combined in this study wide-angle x-ray scattering (WAXS), transmission electron microscopy (TEM) with related analytical techniques such as energy dispersive spectroscopy (EDS), extended x-ray absorption fine structure (EXAFS), x-ray photoelectron spectroscopy (XPS) and transmission ^{57}Fe Mössbauer spectrometry. The magnetic properties of the Fe-Bi nanospheres were also measured using a superconducting quantum interference device (SQUID).

Experimental section

Synthesis

General methods

All operations (material preparation, sampling and packaging) were carried out using standard Fischer-Porter bottle techniques and glove-box under argon. $Fe(N(SiMe_3)_2)_2$ (>99%) was purchased from Nanomeps and anhydrous anisole from Sigma-Aldrich. Anisole was purified by distillation under argon (over sodium) and further degassed by the freeze-pump-thaw technique and finally dried over molecular sieve (0.4 nm) before use. $Bi(N(SiMe_3)_2)_3$ [21] and iPr_2NH-BH_3 [22] were prepared and purified according to published procedures. Dihydrogen was purchased from Air Liquide and contained less than 3 ppm of H_2O and 2 ppm of O_2. To determine the Fe and Bi contents in the materials, elemental analyses were performed at Antellis [23] by ICP-MS (Inductively Coupled Plasma-Mass Spectrometer), after digestion of the samples in concentrated HNO_3.

Sample preparation

$Fe(N(SiMe_3)_2)_2$(80 mg, 0.21 mmol), $Bi(N(SiMe_3)_2)_3$ (20mg, 0.03 mmol), *HMDS* (343 mg, 2.1 mmol) were dissolved in anisole (18 mL, H_2O < 3ppm) in a Fischer-Porter bottle in a glove box. The homogeneous yellow-green solution was freezed under liquid nitrogen and 1.1 equivalent of diisopropylamine-borane with respect to iron (27 mg, 0.24 mmol) in anisole (4 mL) were canula-

transferred in the Fischer-Porter bottle. Slow warm-up of the reaction medium up to room temperature afforded a dark brown solution. This homogeneous solution was then pressurized under 3 bar H_2 and heated 4h at 110°C and 19h at 150°C without any stirring. A black magnetic solid was recovered by filtration, washed with anisole (5 mL) and dried under vacuum (recovered mass: 16mg; Fe: 11.18% ; Bi: 5.52 % i.e. atomic composition $Fe_{7.6}Bi_1$). The same procedure was repeated and the reaction stopped at different reaction times to investigate the evolution of the material: before pressurization under H_2, after 4h at 110°C, after 4 and 72h hours at 150°C.

WAXS and EXAFS experiments

The samples for WAXS experiments consisted in small amounts of the pure powders sealed in 1 mm Lindemann glass capillaries. Measurements were performed using a dedicated two-axis diffractometer equipped with a graphite flat monochromator in order to select the molybdenum K_α wavelength (0.07107 nm). A solid-state detector was used to discriminate scattering from Fe and Bi intense fluorescence radiations. Data sets typically included 457 measurements in the range $0^\circ \leq \theta \leq 65^\circ$ for equidistant s values $[s = 4\pi(sin\theta/\lambda)]$. Measurement time was typically 15 hours for each sample.

X-ray absorption (XANES and EXAFS) experiments were performed on beamlines C and X1 of Hasylab synchrotron facility at HASYLAB in Hamburg. For each composition, two samples were prepared by compacting a pellet of the powder mixed with the appropriate amount of poly(2,6-dimethyl-p-phenylene) oxide (PPO) in order to have optimal absorption at Fe K-edge (7112eV) or Bi L_3-edge (13419eV). The measurements were done in transmission mode at room temperature using a Si(111) double monochromator. Metal foils were measured simultaneously in the monitor position for accurate energy calibration. The EXAFS signal was extracted using the Athena program and structural parameters were refined using the Artemis program.[24]

TEM and EDS experiments

Samples for TEM experiments were dispersed in toluene or anisole previous to deposition on ultrathin carbon films supported by a lacey carbon film on a 400 mesh copper grid. They were exposed to air just before their introduction in the microscope. The samples were analyzed using a Cs-corrected Tecnai F20 and a CM20 FEI microscopes. Both microscopes are fitted with a field emission gun. Elemental mapping of isolated particles was performed by energy dispersive x-ray spectroscopy (EDS) to address compositional variations from the core to the surface of the particles. The EDS spectra were recorded in STEM mode on the CM20, which is fitted with a Bruker QUANTAX EDS system.

XPS experiments

Samples for XPS experiments were prepared in an ultra-pure atmosphere (within the argon glove-box directly connected to the spectrometer) and mounted on a stainless sample holder using conductive copper tape. Surface elemental and chemical state analyses were performed on a $K\alpha$ x-ray photoelectron spectrometer (Thermo Scientific). This instrument is equipped with a micro-focusing monochromator (Al-$K\alpha$ x-ray source at 1486.6 eV), which was operated at a spot size of 400 μm diameter, and a pass energy of 20 eV. The spectrometer was calibrated using the photoemission lines of Au (Au4$f_{7/2}$ = 83.9 eV, with reference to the Fermi level) and Cu (Cu2$p_{3/2}$ = 932.5 eV); for the Au4$f_{7/2}$ line, the full width at half maximum (FWHM) was 0.86 eV in the recording conditions. Charge effects were compensated by the use of a dual-beam charge neutralisation system (low energy electrons [typically 1.85 eV] and Ar^+ ions) which had the unique ability to provide consistent charge compensation. All the neutraliser parameters remained constant during analysis. For the study, charge referencing was done against adventitious carbon (C1*s* binding energy = 284.6 eV). Spectra were analyzed and mathematically described using CasaXPS software. The XPS signals were analysed by using a least squares algorithm and a non-linear baseline. The fitting peaks of the experimental curves were defined by a combination of gaussian (70 %) and lorentzian (30 %) distributions.[25]

Mössbauer experiments

The samples for Mössbauer analyses consist of a thin layer containing about 5 mg of Fe per cm^2 of FeBi powders dispersed in PPO that was sealed in glove box with inert atmosphere to avoid oxidation. ^{57}Fe Mössbauer spectra were recorded using a ^{57}Co/Rh γ-ray source mounted on a conventional electromagnetic drive using a triangular velocity form. They were obtained at 77K, 300 K without external magnetic field and at 10 K in an 8 T field oriented parallel to the γ-beam. The Mössbauer spectra were analysed using the 'MOSFIT'.[26] The hyperfine structure was modelled by a least-square fitting procedure involving Zeeman sextets composed of either lorentzian or gaussian lines. The isomer shift values (IS) were referred to that of the α-Fe at 300 K.

SQUID experiments

Hysteresis loops were recorded at 2 K, between -5 T and +5 T using a MPMS Quantum Design SQUID. The as-prepared powder was sealed in a gelatin capsule to prevent any oxidation during the transfer of the sample into the magnetometer. Elemental analysis was carried out directly on the capsule to enable normalisation of the magnetization with respect to the Fe content in the sample.

Results and discussion

A core-shell chemical distribution

Structure and morphology

TEM observations give evidence for the presence of only one type of particles: nanospheres with a mean diameter 150 $\pm$ 30nm, as determined from the analysis of about one hundred particles. A typical TEM image is displayed in Figure 1. The enlarged view of a nanosphere shows that it is composed of numerous small grains about 2 to 3 nm large, at least at the surface region thin enough to present electron transparency. The core-shell contrast observed in such large particles cannot be readily attributed to a difference in chemical composition as it is also the expected contrast for a

spherical object, the thicker region of the core being much more absorbent for the incident electron beam than the surface region.

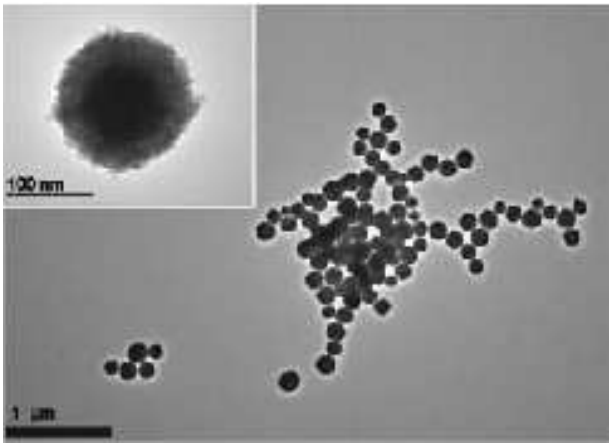

Figure 1: TEM image of the Fe-Bi nanoparticles. An enlarged view of one particle, revealing the presence of numerous nanograins, is displayed in inset.

In order to check the compositional variation across the nanospheres and in particular from core to surface, several nanospheres were examined using spatially resolved STEM-EDS with an electron probe size of 2 nm. Spectrum images were recorded using a drift correction and further processed for quantitative analysis of the different elements. Figure 2 presents the elemental mapping data for an ensemble of three particles, which provides clear evidence for a compositional variation from shell to core: the shell seems to be mainly composed by iron while most of the bismuth content seems concentrated in the particle core. The quantitative analysis of the displayed group of particles gives a Fe/Bi ratio of $Fe : Bi = 0.875/0.125 = 7$, remarkably close to the nominal ratio introduced at the beginning of the synthesis. Analyses performed on spectrum images of different particles gave very close results, the ratio remaining in the range 7 ± 0.25. The compositional gradient from surface to core of the nanospheres is better evidenced when the atomic composition is plotted along a line profile taken across a nanosphere diameter. Such a plot is displayed as supporting information (figure SI1). Clearly, the ratio of the different elements strongly differ in the surface and in the core of the nanosphere. Of course, while the displayed surface region is effectively representative of the shell, the spectra recorded in the central part of the nanospheres include both the contribution from the particles core and the contribution from top

and bottom regions of the shell. The shell composition, analyzed from small regions taken in the surface region, is thus estimated to $Fe/Bi = 93.6/6.4 = 14.625$. The composition of the core was then deduced from the two known compositions, i.e. mean composition and shell composition, using a simple model of a spherical particle fully occupied by Fe and Bi atoms with different atomic volumes. Such estimation gives a Fe/Bi ratio slightly less than 1. One can conclude from these analyses that the observed nanospheres are fully representative of the whole sample as they seem to gather all the metallic atoms introduced in the synthesis. The core of the nanospheres, with a volume about 5 times smaller than the shell, has a composition close the $Fe/Bi = 1/1$ (i.e; around 50% of Bi) while the shell includes only 6.4% of Bi. However, nothing can be said at this step about the distribution of the different metals in these regions, and in particuler about the possible formation of metastable Fe-Bi alloys at this nanometer scale.

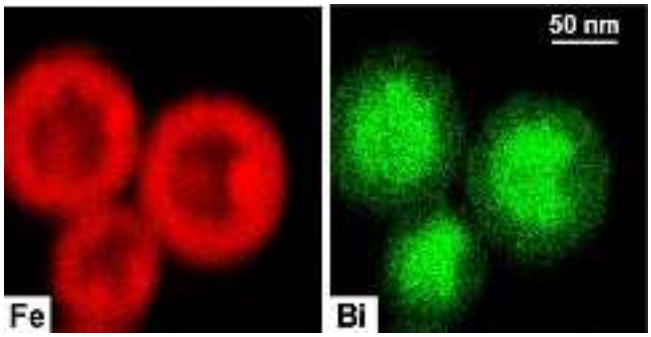

Figure 2: Local elemental mapping of Fe-Bi nanospheres giving evidence for an iron-rich shell and a concentration of Bi atoms in the core region (intensity corresponds to counts).

The observed core-shell distribution is not the one expected from both thermodynamic and kinetic considerations. Bismuth has a much lower surface energy than iron ($0.537 J.m^{-2}$ for Bi compared to $2.222 J.m^{-2}$ for Fe)[27] as well as a much larger atomic size. These two parameters should promote a segregation of bismuth at the surface of the nanospheres owing to energy minimization considerations. Moreover, the synthesis procedure itself was designed to ensure the sequential decomposition of the two different precursors. Indeed, control experiments (detailed in SI) revealed that the bismuth precursor is very stable and requires a temperature as high as 150°C to be decomposed under dihydrogen, while the reduction of the iron precursor in the presence of amine-borane is quasi-instantaneous at the very beginning of the process carried out close to -40°C. In order to

shed some light on this unexpected chemical distribution, the close atomic environment of the two metals was investigated by different complementary techniques.

A chemical overview of the Fe-Bi compound was first given through XPS analyses. In addition to iron and bismuth, which were both found in a metallic state, the XPS analysis highlights the presence of some traces of light elements coming from metal-organic precursors/HMDS decomposition as well as boron coming from the amine-borane used as reducing agent and easily dehydrogenated. The presence of B-Fe bonds was clearly revealed at the B-1*s* core peak (presented in supporting information, figure SI2). Indeed this peak displayed a small component at 188.2 eV associated with a low atomic percentage of boron (1.2%). This component corresponds to a specific fingerprint of Fe-B bonds recorded from a reference FeB alloy in agreement with a previous work.[28] In light of these results, one can conclude that boron, coming from the amine-borane reducing agent, is present in the iron close environment.[29]

X-ray absorption experiments were also carried out at the Fe *K* (7112eV) and Bi L_3 (13419eV) edges. Figure 3 presents the uncorrected Fourier transforms (FT) of the EXAFS functions at both edges together with the references from pure Fe and Bi foils. The FT at Fe edge is consistent with metallic iron, however it significantly differs from the bcc pattern observed for the reference foil: the peak including bonding distances is broad and shifted to shorter distances. Its amplitude is reduced tenfold compared to bulk iron. This points towards an environment for Fe atoms characterized by a strong dispersion, both in bond lengths and chemical species (i.e. including Fe atoms but also lighter elements like C, N, O and B), however already observed for small iron particles also synthesized by a soft chemical route.[30] Such a disorder is not observed at the Bi edge, but the pattern clearly evidences a mixed environment for Bi atoms. Even if FTs of heavy elements like Bi must be considered carefully (e.g., the broad asymetrical peak for the Bi foil is actually related to a single well defined bonding distance), there is no real ambiguity : the longer distance (0.3 nm, uncorrected) is related to a metallic Bi environment, but the shorter one (0.22 nm) points to a different backscattering atom. Considering both atom size and phase shift, this indicates that in the whole sample, a large part of Bi atoms have Fe neighbours.[31] Here also, very light elements

like C, N, O and B cannot be excluded but should only marginally contribute to the left side of the main peak. Metallic bonding between Bi and Fe atoms should also be observed at Fe edge, and actually the right side of the main peak may include such a contribution, however quite low for two reasons: the low percentage of Bi in the material, but also the high static disorder in Fe neighbouring already reported. Since the relatively short Fe-Fe bond is already largely suppressed, an even more dramatic effect is expected in these conditions for the longer Fe-Bi one. The EXAFS results thus agree with a mixed Bi and Fe environment for Bi atoms. As most of the iron atoms are located in the bismuth poor shell region of the nanospheres (the shell volume is 5 times larger than the core volume and contains nearly 94% of iron), the observed Fe-Bi bonds at the Bi edge most probably originate from the core region whose composition was previously estimated close to $1/1$. The fact that both Fe-Bi and Bi-Bi bonds exist gives a strong indication for the presence of pure Bi nanograins in the core region together with Fe-Bi alloy and possibly also pure Fe grains.

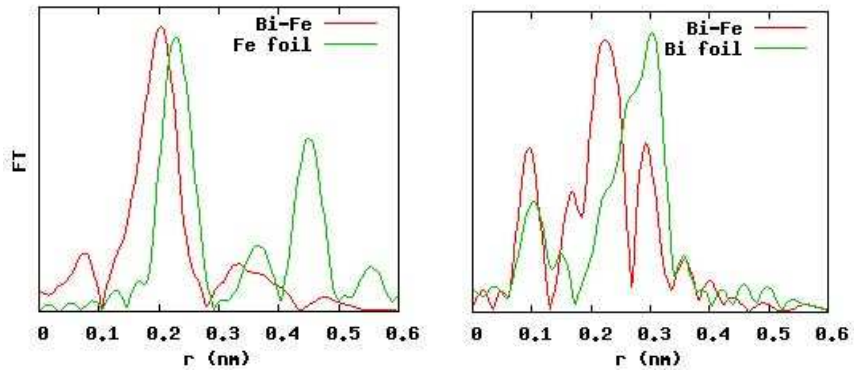

Figure 3: Magnitudes of uncorrected Fourier transforms at Fe K edge (left) and Bi L_3 edge (right). For easier comparison, the reference foils were adjusted using a scaling factor (0.10 and 0.80 for Fe and Bi, respectively).

The local environment of Fe was further analyzed through Mössbauer spectroscopy experiments. The zero field ^{57}Fe Mössbauer spectrum collected at 77K displays a pure magnetic sextet composed of asymmetrical broadened lines (figure SI3 in Supporting Information). The broadening of the lines probably results from the chemical inhomogeneity. Different fitting models were attempted to describe the hyperfine structure, assuming either one or two magnetic components with distribution of hyperfine fields and lorentzian or gaussian lines. The best agreement, in par-

ticular for the fit of the inner lines, was obtained when considering 2 magnetic components with gaussian lines and independent linewidths. However the solution involving two discrete distributions of hyperfine fields was preferred as the gaussian profile is not physically appropriate.The mean hyperfine field and isomer shift values are estimated at about 26 and 33T, 0.23 and 0.18 mm/s, respectively, while the quadrupolar shift values remain close to zero (see table 1). The results agree with the occurrence of two different environments for iron (consistently with XPS). The low and broadened hyperfine field component can be attributed to Fe atoms surrounded by B atoms: indeed, investigation of crystalline and amorphous Fe borides reveals that the hyperfine field at ^{57}Fe sites highly depends on the presence of boron atoms as first neighbours, with values ranging from 20 to 25T at 77K.[32] In addition, the increase of the isomer shift up to about 0.25-0.30 mm/s at 77K is also nicely consistent with the presence of B species in the close vicinity of Fe.[33] On the other hand, the high hyperfine field component is most probably due to rather pure Fe disordered phase taking account of the observed line broadening (let us recall that the hyperfine field value in the well-ordered α-Fe phase is 33.7 T at 77K). The present situation appears to be rather consistent with that observed in grain boundaries of nanocrystalline Fe materials resulting from in situ consolidated Fe clusters generated by inert gas condensation.[34] Consequently, the hyperfine structure of present Fe-Bi nanospheres should result from combined effects including the presence of boron, the disordered topological structure and the surface or interface effects which contribute also to disturb the local environment of ^{57}Fe probes. Such a complexity prevents from an estimation of the boron content diffused into the iron clusters. The lack of reference on the Fe-Bi immiscible system prevents further analysis on the presence of Bi in the Fe environment.

Table 1: - Comparison between refined values at 77K of hyperfine parameters (mean isomer shift $< \delta >$ and mean hyperfine field $< B_{hyp} >$) obtained by means of different fitting procedures involving gaussian and lorentzian profiles, G and L respectively.

Sub-spectrum	$< \delta > (mm.s^{-1})$ ± 0.01	$< 2\varepsilon > (mm.s^{-1})$ ± 0.01	$< B_{hyp} > (T)$	Area $(1)/(2)$ ± 0.01
(1) G / L	0.19 / 0.18	-0.02 / -0.00	32.2 / 33.0	67 / 57
(2) G / L	0.32 / 0.23	-0.01 / 0.1	25.5 / 26.0	33 / 43

Properties

Despite the presence of iron in the shell, the nanospheres display good magnetic properties and resistance to oxidation during air exposure. Figure 4 shows the hysteresis loops recorded by SQUID experiments on both fresh (directly after synthesis) and aged (after 1 day of air exposure) Fe-Bi samples, the magnetization being normalized with respect to the iron content. The fresh sample displays an enhanced magnetization compared to bulk iron (234 $A.m^2/kg$ to be compared with 218 $A.m^2/kg$). Such an enhancement was already observed in 2nm-wide Fe nanoparticles stabilized in a polymer displaying a poorly ordered polytetrahedral atomic arrangement, and was attributed to strong surface effects in so small particles.[35] After air exposure, the magnetization remains high, typically at 92.2% of its value in bulk iron, which represents a decrease of 14% compared to the fresh specimen.

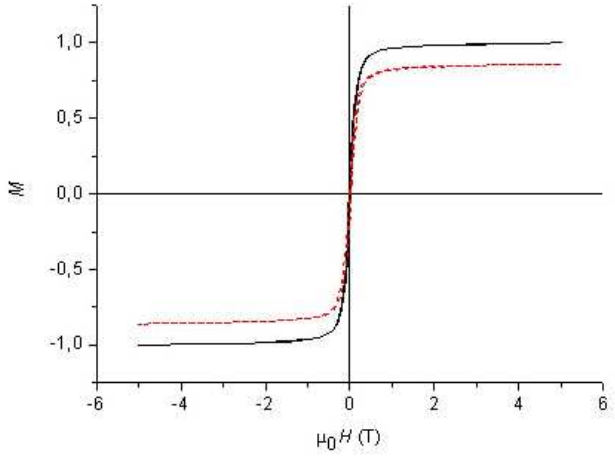

Figure 4: Hysteresis loops of the Fe-Bi nanospheres recorded just after the synthesis (black solid line) and after 24 hours of air exposure (red dotted line).

The comparison of Mössbauer spectra obtained at 77 K on the as-prepared powder and after about 4 months ageing however revealed significant changes, which can be attributed to an evolution of the Fe-Bi nanospheres. The difference essentially comes from the narrowing of lines which can be assigned *a priori* to some local atomic reordering. Further Mössbauer spectra were performed at 300K (without external field) and at 10K (under 8T external field) on aged samples to better understand the atomic scale Fe surroundings and the magnetic orientation of magnetic

Fe moments (figure 5). The in-field Mössbauer spectrum consists of only 4 broadened and asymmetrical lines: the disappearance of the intermediate lines indicates unambiguously that the Fe magnetic moments are aligned parallel to the γ-beam, making thus easier the hyperfine structure. As the applied field is parallel to the γ-beam, in the cryomagnetic device, one should conclude to a ferromagnetic structure; in addition, the reduction of the magnetic splitting compared to that of the zero-field spectrum suggests that the hyperfine field is opposite to the magnetic moment. The same fitting model involving distribution of magnetic components was applied at both 300K and 77K, and at 10K under external magnetic field, in order to ensure a suitable determination of the mean value of the canting angle. The effective field (equivalent to the vectorial sum of both applied field and hyperfine field) distribution, established from the in-field spectrum, allows us to estimate the hyperfine field distribution taking into account both the canting angle and the applied field values. The hyperfine field distributions are compared in figure 5 (right) : one observes clearly a refinement of both components, particularly the low field one, with decreasing temperature. A summary of the values of hyperfine parameters is given in table 2. The refined values of isomer shift are consistent with the presence of metallic Fe species. In addition, the in-field Mössbauer spectrum fairly agrees with the presence of a ferromagnetic structure with reference to both the early observations by Hanna *et al.*[36] and the low canting angle. All these results suggest an evolution of the sample with time. As we cannot exclude some air exposure during the samples transfer and residual oxygen exposure during the long stay in the glove box, the observed evolution (atomic reordering, ferromagnetic metallic iron) could be attributed to the migration of some interstitial (or substitutional) boron atoms from the volume of the iron nanograins to their surface so as to form a protective boron oxide. This scenario is also supported by the observation of boron oxide in XPS analyses of aged specimens. The role of bismuth in the observed properties remains unclear. However, enhanced resistance to oxidation and good magnetic properties were reported in Fe-Bi alloys examined by Forester and co-workers[16] and our EXAFS experiments strongly suggest the formation of an Fe-Bi amorphous alloy, at least in the core of the nanospheres. Further analyses will be necessary to gain full understanding of the different parts played by these elements but

the good resistance to oxidation of these bi-metallic core@shell compounds together with the low biological toxicity of bismuth made these compounds particularly valuable for further applications in biology.[37]

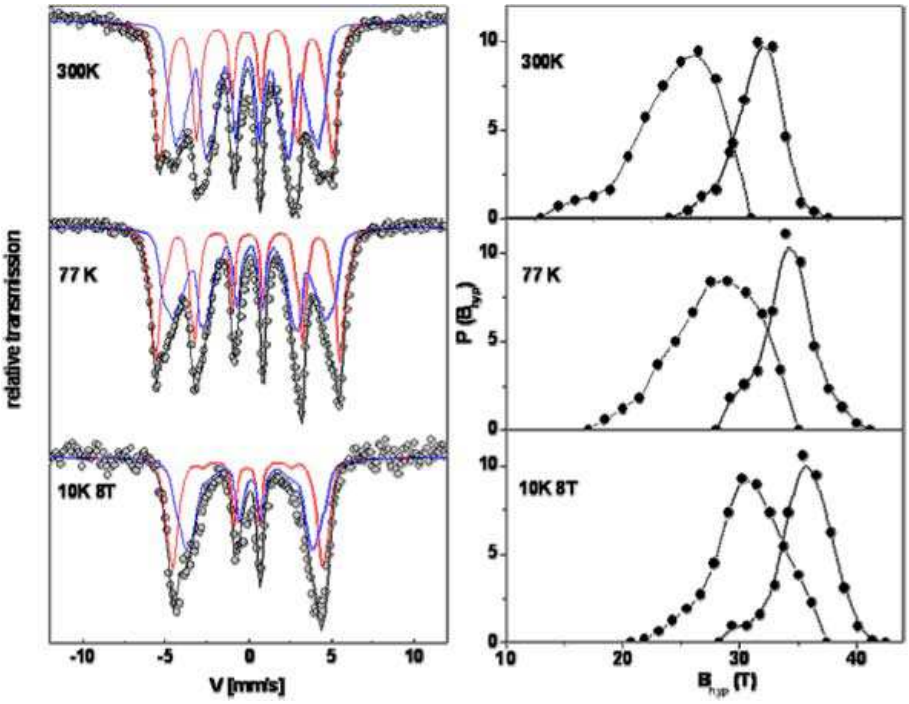

Figure 5: ^{57}Fe Mössbauer spectra obtained at 300 K, 77 K (without external magnetic field) and 10 K in 8 T magnetic field applied parallel to the γ-beam on powder after 4 months (left side). Spectrum and sub-spectra result from distribution of magnetic sextets based Lorentzian lines which are represented on right side.

Origin of the formation of Bi@Fe nanospheres

In order to understand the origin of the unexpected core@shell distribution, and thus to provide a better control of the synthesized samples, we analyzed the different stages of the formation of the Fe-Bi nanospheres by collecting samples at the main steps of the synthesis sequence, as sketched in Figure 6. The different samples are numbered from S1 to S5, the previously observed Fe-Bi nanospheres corresponding to sample S4 in the sequence.

The XPS analysis of the two precursors, $Fe(N(SiMe_3)_2)_2$ and $Bi(N(SiMe_3)_2)_3$ was undertaken in order to precise the binding energy (BE) of Fe-2p and Bi-4f core peaks in these compounds.

Table 2: - Summary of refined values of hyperfine parameters obtained at 300 K, 77 K and 10 K (mean isomer shift $<\delta>$, mean quadrupolar shift $<2\varepsilon>$, mean canting angle $<\theta>$ and mean hyperfine field $<B_{hyp}>$).

	$<\delta>(mm.s^{-1})$ ± 0.01	$<2\varepsilon>(mm.s^{-1})$ ± 0.01	$<\theta>$ $(^{\circ}\pm 10$	$<B_{hyp}>(T)$ ± 2	Area $(1)/(2)$ ± 0.02
300 K (1)	0.04	-0.03	-	32.0	0.41
(2)	0.10	-0.04	-	25.0	0.59
77 K (1)	0.13	-0.01	-	34.0	0.43
(2)	0.22	-0.02	-	28.0	0.57
10 K (1)	0.14	0.04	15	35.6	0.44
(2)	0.29	0.00	20	31.0	0.56

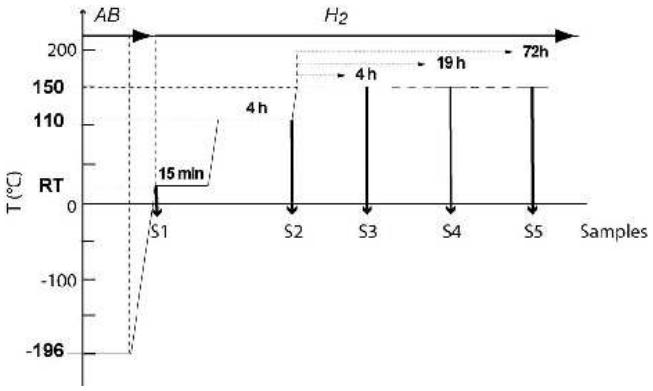

Figure 6: Sketch of the synthesis sequence and samples collected at the different steps, numbered from S1 to S5.

For bismuth, besides a Bi-4f doublet characteristic of an oxygenated environment of bismuth (BE $Bi-4f_{7/2}$ 159.0eV) a small $Bi-4f_{7/2}$ component appears at 158.0 eV. This BE is in line with the value reported in a recent paper for Bi-N bonds in Bi-Fe(N) layer.[38] This result shows that the signature of Bi in the precursor is clearly different from Bi metal (BE $Bi-4f_{7/2}$ at 159.0 eV). For $Fe(N(SiMe_3)_2)_2$ it was not possible to precise the signature of Fe according to the well known reactivity of this precursor with traces of water favoring the occurrence of FeO nanoparticles.[39] Figure 7 presents high resolution spectra of Bi-4f and Fe-2p ionization peaks at different steps of the synthesis (samples $S1$, $S2$ and $S4$). The Bi-4f peak displays, on all the spectra, a well-defined $4f_{7/2-5/2}$ doublet at 157.0eV-162.2eV, significant of the decomposition of the $Bi(N(SiMe_3)_2)_3$ precursor. The decomposition of the bismuth precursor at the very beginning of the synthesis (sample $S1$) while Bi was expected to be reduced by dihydrogen at 150 °C only, is certainly an important information. In parallel, the iron ionization peak shows a slow evolution from $S1$ to $S4$. Iron is essentially in an oxidized state at room temperature while a strong metallic iron component arises only during step 2, i.e. after 4 hours under dihydrogen at 110°C. Sample $S3$ (not shown here) still contains an important proportion of iron in an oxidized state. Finally, the Fe-2p peak displays a $2p_{3/2-1/2}$ doublet at 707.1eV-720.3eV, clearly assigned to a non-oxidized environment, after 19h at high temperature in the $S4$ sample. The oxidized state of iron observed in the previous steps of the synthesis is probably related the adventitious hydrolysis of the Fe amido-complex, still present in $S1$ to $S3$ samples during sample preparation for XPS. Finally, XPS analyses of the $S5$ specimen (not shown) are similar to the $S4$ ones.

These results allow to conclude that the simultaneous presence of the two precursors in the solution definitely favors the bismuth precursor decomposition. In other words, the zero-valent Fe atoms resulting from the fast reduction of the iron precursor in the presence of amine-borane, induce the subsequent reduction of the bismuth precursor according to a redox process which can be summarized as follows,

$$3\mathrm{Fe}^0 + 2Bi(N(SiMe_3)_2)_3 \longrightarrow 3Fe(N(SiMe_3)_2)_2 + 2\mathrm{Bi}^0$$

clearly regenerating the Fe precursor in the reacting medium as long as there is still some

bismuth precursor to reduce. In this first step of the reaction, the Fe amido complex acts as a catalyst for the reduction of the bismuth amido one. The bismuth precursor is soon completely decomposed (the Fe/Bi ratio is equal to 7.6) and the iron molecular species released in the solution become stable and can grow to form nanoparticles.

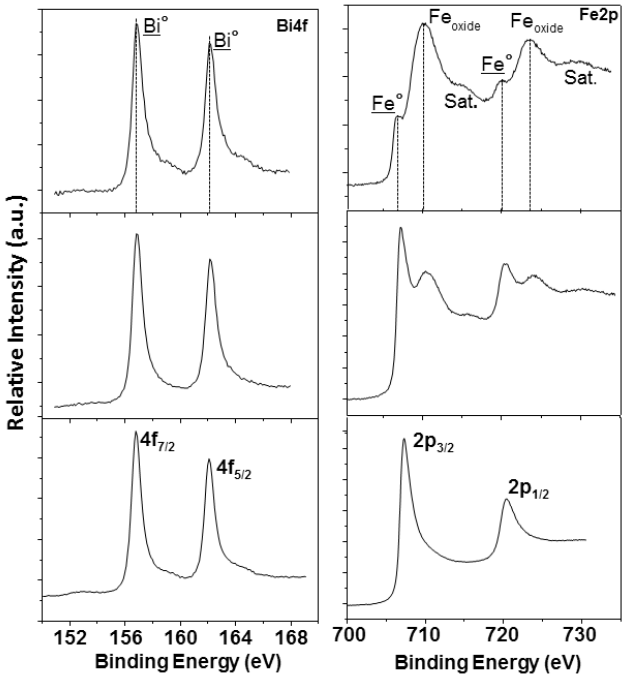

Figure 7: Evolution of the XPS spectra in the Bi-4f and Fe-2p regions through the different steps of the synthesis. Top: sample *S*1 in the presence of amine-borane, middle: sample *S*2 after 4h at 110°C under dihydrogen, bottom: sample *S*4 after 19h at 150°C under dihydrogen- underlined symbols were chosen for Bi° and Fe° to include Bi-Fe, respectively Fe-Bi, bonds in the pure metals peaks.

The same sequence of samples was analyzed using WAXS and EXAFS. WAXS could be applied to all steps of the synthesis and provides insight to the average structure. On the left of Figure 8 (reciprocal space), the prominent feature is a broad amorphous pattern from *S*1 to *S*4. *S*5 is dominated by the rhombohedral Bi pattern, which gives evidence of the formation of extended Bi crystals (several nanometers) in this last step. The Radial Distribution Function (RDF) on the right of Figure 8 provides more information: from *S*1 to *S*3, well defined distances point to a phase quite different from both iron and bismuth. Since amplitudes in the RDF are strongly related to the atomic numbers of atoms engaged in the pair, we can expect distances related to Bi atoms to

retain a large amplitude even for a relatively low concentration of the metal. Actually, the main peak located at 0.27 nm points to a distance (indicated by a vertical bar) quite consistent with a Bi-Fe bond. At the next step, *S*4, the peak at this distance strongly decreases and at *S*5 we can mostly observe the single Bi-Bi bonding distance at 0.31 nm, the following distances being also in agreement with the structure of bulk bismuth. This clearly indicates that an amorphous material including Bi appears very early in the synthesis and that the production of pure metallic bismuth crystals is a long process.

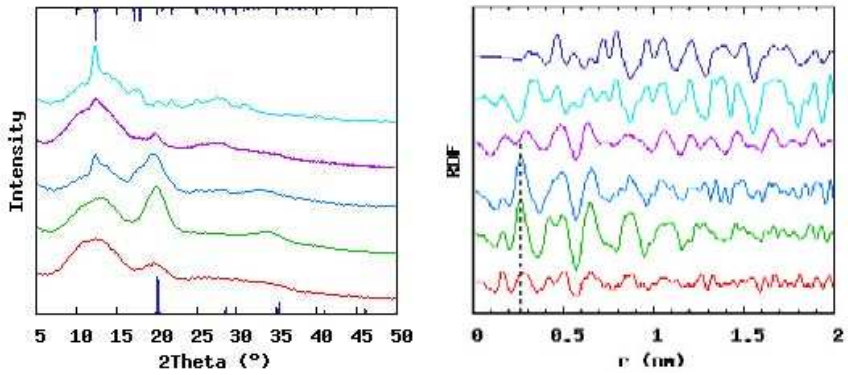

Figure 8: Evolution from bottom to top *S*1 to *S*5; left: in reciprocal space - bottom axis, bcc Fe pattern, reverse top axis Bi pattern; right: in real space - on top, simulation from bulk Bi.

EXAFS was also performed on all samples excepted *S*5, as it provides the unique ability to investigate short range order for both metals. Figure 9 presents the evolution of the uncorrected Fourier Transforms (FT) of the EXAFS functions at both edges. Study at Fe *K* edge provides limited information: at all steps, only one broad peak can be observed. One major change can however be observed: for *S*1, the broad peak points to still shorter distances, which indicates that it includes a higher amount of bonding distances between Fe and light elements, in agreement with the fact that iron could be mostly in a molecular state, as expected if a transmetalation process occurs in the first stages of the reaction. Study at the Bi edge clearly evidences the process: the peak at 0.22 nm (uncorrected), already noticed in the previous section, can be observed from *S*1 and already points to Fe in Bi environment. At this step, there is no evidence of pure Bi. The minor peak at 0.17 nm (uncorrected) points to a distance between Bi and a light element, which could correspond to some remaining bismuth precursor although this is not supported by the XPS

analyses. At *S*2, we observe the growth of the Bi alloy and a strong decrease of the peak at 0.17 nm. At *S*3, this Fe-Bi material is the only phase including bismuth in the sample. A least-square refinement was performed on this spectrum and very good agreement was obtained with a single Bi-Fe distance at 0.274 nm (figure SI4 in supporting information). At *S*4, we can see that the Bi-Fe peak decreases and the Bi-Bi one finally appears, in agreement with WAXS investigations. This evolution clearly indicates that the mixed environment observed for Bi atoms in the initial sample *S*4 is actually related to a mixture of pure metallic Bi with an amorphous Fe-Bi alloy. The precise composition of this Fe-Bi alloy cannot be estimated from our analyses, despite the large range of techniques implemented in this study. However, in their study of Fe-Bi films grown at room temperature by electron-beam deposition, Forester *et al.* [16] showed that the most stable alloys formed for a Bi concentration around 20%. Besides, the magnetic moment per iron atom in this alloy was found to reach at least 95 % of its value in bcc iron. Solid solutions with higher or lower Bi content were seen to undergo phase separation with the formation of pure iron or bismuth nanocrystals. It seems therefore reasonable to assume a 20% Bi content in the observed Fe-Bi alloy. According to the STEM-EDS analyses, the nanospheres core contains 50% bismuth, which strongly suggests that all the pure Bi nanograins are concentrated in this region together with the iron rich amorphous alloy. The weak Bi content (around 6%) evidenced in the shell region could remain in between Fe particles which were found to include some boron interstitial or substitutional atoms, at least in fresh specimens.

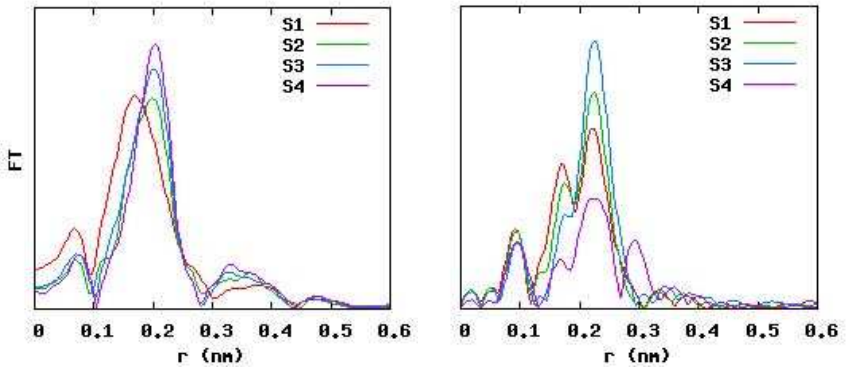

Figure 9: Evolution of the magnitudes of uncorrected Fourier transforms from *S*1 to *S*4 at Fe *K* edge (left) and Bi *L*3 edge (right) - for each edge, all curves are plotted at the same scale.

Conclusion

We have developped the synthesis of bimetallic Fe-Bi particles in the non-miscible Fe-Bi system. A clear description of these particles and their properties was obtained through the use of complementary techniques as STEM-EDS, WAXS, EXAFS, XPS and Mössbauer spectrometry. The particles, 150 nm of mean diameter, present a core@shell chemical order with a bismuth rich core and a shell formed by an assembly of 3 nm large iron nanoparticles. Such a chemical order, which was fully unexpected from both thermodynamic and kinetic considerations, has been explained through the analyses of the compound by XPS, WAXS and EXAFS experiments at different stages of the synthesis. Evidence has thus been given for the occurrence of a transmetalation process in these compounds, which occurs at the very first stages of the synthesis and favours the formation of an Fe-Bi amorphous alloy. When the Fe-Bi particles are formed, this alloy remains concentrated at their core together with pure bismuth grains. To our knowledge this is the first evidence for the formation of a Fe-Bi alloy in nanomaterials and using a soft chemistry route. Finally, we demonstrated the enhanced resistance to oxidation in these particles, despite their shell mainly formed by Fe nanoparticles. Good magnetic properties and resistance to air exposure as well as a relative innocuity of bismuth in biology give to these particles a very good potential for multifunctional technological applications .

Acknowledgement

This work has been supported by the ANR, the french National Research Agency (Mag@M project ANR-09-BLAN-0002-01). The research leading to these results has received funding from the European Community's Seventh Framework Programme (FP7/2007-2013) under grant agreement nř 312284. The EXAFS experiments were carried out at the light source DORIS III at DESY, a member of the Helmholtz Association (HGF). We would like to thank Roman Chernikov for assistance in using beamline C and Edmund Welter in using beamline X1, as well as A. Mari and L. Rechignat for their help in SQUID measurements.

Supporting information available

The four figures referred in the text as SI1, SI2, SI3 and SI4 are available as supporting information, together with details on the control experiments with the iron and bismuth precursors. This information is available free of charge via the Internet at http://pubs.acs.org.

Notes and References

(1) Cozzoli, P. D.; Pellegrino, T.; Manna, L. *Chem. Soc. Rev.* **2006**, *35*, 1195–1208.

(2) Wang, H.; Brandl, D. W.; Le, F.; Nordlander, P.; Halas, N. J. *Nano Letters* **2006**, *6*, 827–832.

(3) Zeng, H.; Sun, S. *Advanced Functional Materials* **2008**, *18*, 391–400.

(4) Bao, Y.; Calderon, H.; Krishnan, K. M. *The Journal of Physical Chemistry C* **2007**, *111*, 1941–1944.

(5) Becker, J.; Zins, I.; Jakab, A.; Khalavka, Y.; Schubert, O.; Sönnichsen, C. *Nano Letters* **2008**, *8*, 1719–1723, PMID: 18454558.

(6) Zitoun, D.; Respaud, M.; Fromen, M.-C.; Casanove, M. J.; Lecante, P.; Amiens, C.; Chaudret, B. *Phys. Rev. Lett.* **2002**, *89*, 037203.

(7) Cho, S.-J.; Shahin, A. M.; Long, G. J.; Davies, J. E.; Liu, K.; Grandjean, F.; Kauzlarich, S. M. *Chemistry of Materials* **2006**, *18*, 960–967.

(8) Park, H.-Y.; Schadt, M. J.; Wang,; Lim, I.-I. S.; Njoki, P. N.; Kim, S. H.; Jang, M.-Y.; Luo, J.; Zhong, C.-J. *Langmuir* **2007**, *23*, 9050–9056.

(9) Sun, Q.; Kandalam, A. K.; Wang, Q.; Jena, P.; Kawazoe, Y.; Marquez, M. *Phys. Rev. B* **2006**, *73*, 134409.

(10) Naitabdi, A.; Ono, L. K.; Behafarid, F.; Cuenya, B. R. *The Journal of Physical Chemistry C* **2009**, *113*, 1433–1446.

(11) Heremans, J. P.; Thrush, C. M.; Morelli, D. T.; Wu, M.-C. *Phys. Rev. Lett.* **2002**, *88*, 216801.

(12) Lin, Y.-M.; Cronin, S. B.; Ying, J. Y.; Dresselhaus, M. S.; Heremans, J. P. *Applied Physics Letters* **2000**, *76*, 3944–3946.

(13) Yang, F. Y.; Liu, K.; Chien, C. L.; Searson, P. C. *Phys. Rev. Lett.* **1999**, *82*, 3328–3331.

(14) Wang, W. Z.; Poudel, B.; Ma, Y.; Ren, Z. F. *The Journal of Physical Chemistry B* **2006**, *110*, 25702–25706, PMID: 17181209.

(15) Cui, F. Z.; Fan, Y. D.; Wang, Y.; Vredenberg, A. M.; Draaisma, H. J. G.; Xu, R. *Journal of Applied Physics* **1990**, *68*, 701–704.

(16) Forester, D. W.; Schelleng, J. H.; Lubitz, P.; D'Antonio, P.; George, C. *Journal of Applied Physics* **1982**, *53*, 2240–2242.

(17) Chen, Q.-M.; Cui, F.-Z.; Fan, Y.-D.; Li, H.-D. *Journal of Applied Physics* **1988**, *63*, 2452–2453.

(18) Hsu, J.-H.; Wang, H.-X.; Sun, A.-C.; Kuo, P.-C. *Journal of Applied Physics* **2006**, *99*, 08F106.

(19) Mattei, J.; Pelletier, F.; Ciuculescu, D.; Lecante, P.; Amiens, C.; Casanove, M. J. *Journal of Nanoscience and Nanotechnology* **2011**, *in press*.

(20) Ciuculescu, D.; Amiens, C.; Respaud, M.; Falqui, A.; Lecante, P.; Benfield, R. E.; Jiang, L.; Fauth, K.; Chaudret, B. *Chemistry of Materials* **2007**, *19*, 4624–4626.

(21) Vehkamaki, M.; Hatanpaa, T.; Ritala, M.; Leskela, M. *J. Mater. Chem.* **2004**, *14*, 3191–3197.

(22) Green, I. G.; Roberts, B. P. *J. Chem. Soc., Perkin Trans. 2* **1986**, 1597–1606.

(23) `http://www.antellis.com`.

(24) Ravel, B.; Newville, M. *Journal of Synchrotron Radiation* **2005**, *12*, 537–541.

(25) Different standard compounds were analyzed as references in order to precise some attributions: B_2O_3 material from Aldrich (CAS number 1303-86-2); FeB from READE (CAS number: 11108-67-1); FeSi from READE (CAS Number: 8049-17-0), HMDS from Aldrich (CAS number: 99-97-3); SiC from Strem Chemicals (CAS numbers 409-21-2).

(26) Teillet, J.; Varret, F. Mosfit software, Unpublished, Université du Maine.

(27) Vitos, L.; Ruban, A.; Skriver, H.; Kollár, J. *Surface Science* **1998**, *411*, 186 – 202.

(28) Joyner, D. J.; Johnson, O.; Hercules, D. M. *Journal of the American Chemical Society* **1980**, *102*, 1910–1917.

(29) Boron inclusion in Fe nanoparticles is well attested for when borohydride reducing agents are used (see for example, G. N. Glavee, K. J. Klabunde, C. M. Sorensen, and G. C. Hadjipanayis, *Inorganic Chemistry* **34**, 28 (1995). However, no clear proof of such a behaviour is reported for amine-borane reducing agents. As a complementary part of this work, we showed that amine-borane and amino-borane could also lead to the inclusion of boron in Fe seeds. This study is out of the scope of this paper and will be reported separately.

(30) Atamena, N.; Ciuculescu, D.; Alcaraz, G.; Smekhova, A.; Wilhelm, F.; Rogalev, A.; Chaudret, B.; Lecante, P.; Benfield, R. E.; Amiens, C. *Chem. Commun.* **2010**, *46*, 2453–2455.

(31) In principle, Si atoms should also be considered as possible backscattering atoms owing to the position of the shorter distance at 0.22 nm. However, this would imply the decomposition of HMDS, which is quite unlikely owing to the strength of the Si-C bond. This possibility was ruled out during this study as samples synthesized at room temperature (see later samples *S*1 and *S*2) displayed the same kind of environment for Bi while the activation of Si-C bond at room temperature requires the presence of e.g. Pd, Pt, or Ru catalysts.

(32) Barault, G.; Greneche, J. *Solid State Communications* **1995**, *96*, 155 – 160.

(33) Chien, C. L. *Phys. Rev. B* **1978**, *18*, 1003–1015.

(34) Herr, U.; Jing, J.; Birringer, R.; Gonser, U.; Gleiter, H. *Applied Physics Letters* **1987**, *50*, 472–474.

(35) Margeat, O.; Respaud, M.; Amiens, C.; Lecante, P.; Chaudret, B. *Beilstein Journal of Nanotechnology* **2010**, *1*, 108–118.

(36) Hanna, S. S.; Heberle, J.; Perlow, G. J.; Preston, R. S.; Vincent, D. H. *Phys. Rev. Lett.* **1960**, *4*, 513–515.

(37) Andrés-Vergés, M.; del Puerto Morales, M.; Veintemillas-Verdaguer, S.; Palomares, F. J.; Serna, C. J. *Chemistry of Materials* **2012**, *24*, 319–324.

(38) Mai, H.-C.; Hsieh, T.-E.; Jeng, S.-Y.; Chen, C.-M.; Wang, J.-L. *Applied Physics Letters* **2008**, *92*, 021906.

(39) Kahn, M. L.; Glaria, A.; Pages, C.; Monge, M.; Saint Macary, L.; Maisonnat, A.; Chaudret, B. *J. Mater. Chem.* **2009**, *19*, 4044–4060.